Archives of Toxicology (2019) 93:1281–1296
https://doi.org/10.1007/s00204-019-02423-8

MOLECULAR TOXICOLOGY

Interactions of human butyrylcholinesterase with phenylvalerate and acetylthiocholine as substrates and inhibitors: kinetic and molecular modeling approaches

Jorge Estévez[1] · Felipe Rodrigues de Souza[2] · María Romo[1] · Iris Mangas[1,2] · Tanos Celmar Costa Franca[2,3] · Eugenio Vilanova[1]

Received: 5 February 2019 / Accepted: 4 March 2019 / Published online: 15 March 2019
© Springer-Verlag GmbH Germany, part of Springer Nature 2019

Abstract

Phenyl valerate (PV) is a substrate for measuring the PVase activity of neuropathy target esterase (NTE), a key molecular event of organophosphorus-induced delayed neuropathy. A protein with PVase activity in chicken (model for delayed neurotoxicity) was identified as butyrylcholinesterase (BChE). Purified human butyrylcholinesterase (hBChE) showed PVase activity with a similar sensitivity to inhibitors as its cholinesterase (ChE) activity. Further kinetic and theoretical molecular simulation studies were performed. The kinetics did not fit classic competition models among substrates. Partially mixed inhibition was the best-fitting model to acetylthiocholine (AtCh) interacting with PVase activity. ChE activity showed substrate activation, and non-competitive inhibition was the best-fitting model to PV interacting with the non-activated enzyme and partial non-competitive inhibition was the best fitted model for PV interacting with the activated enzyme by excess of AtCh. The kinetic results suggest that other sites could be involved in those activities. From the theoretical docking analysis, we deduced other more favorable sites for binding PV related with Asn289 residue, situated far from the catalytic site ("PV-site"). Both substrates acethylcholine (ACh) and PV presented similar docking values in both the PV-site and catalytic site pockets, which explained some of the observed substrate interactions. Molecular dynamic simulations based on the theoretical structure of crystallized hBChE were performed. Molecular modeling studies suggested that PV has a higher potential for non-competitive inhibition, being also able to inhibit the hydrolysis of ACh through interactions with the PV-site. Further theoretical studies also suggested that PV could yet be able to promote competitive inhibition. We concluded that the kinetic and theoretical studies did not fit the simple classic competition among substrates, but were compatible with the interaction with two different binding sites.

Keywords Human butyrylcholinesterase · Phenyl valerate · Inhibition kinetics · Docking · Molecular dynamics

Abbreviations

AtCh	Acethylthiocholine
ACh	Acethylcholine
AChE	Acetylcholinesterase (in general of any specie)
BChE	Butyrylcholinesterase (in general of any specie)

Jorge Estévez and Felipe Rodrigues de Souza have contributed equally. Tanos Celmar Costa Franca and Eugenio Vilanova contributed equally as directors of the research.

Electronic supplementary material The online version of this article (https://doi.org/10.1007/s00204-019-02423-8) contains supplementary material, which is available to authorized users.

✉ Jorge Estévez
jorge.estevez@umh.es

[1] Institute of Bioengineering, University Miguel Hernández, Elche, Alicante, Spain

[2] Laboratory of Molecular Modeling Applied to the Chemical and Biological Defense (LMCBD), Military Institute of Engineering, Rio de Janeiro, RJ 22290-270, Brazil

[3] Center for Basic and Applied Research, Faculty of Informatics and Management, University of Hradec Kralove, Rokitanskeho 62, 500 03 Hradec Králové, Czech Republic

Ch	Choline
ChE	Cholinesterase (the activity)
hBChE	Human butyrylcholinesterase
MM-PBSA	Molecular Mechanics Poisson Boltzman Solver Area
NTE	Neuropathy target esterase
PV	Phenyl valerate
PVase	Phenyl valerate esterase (the activity)
PDB	Protein data bank

Introduction

Cholinesterases are serine hydrolases present in most living beings capable of processing choline (Ch) esters faster than any other substrate (Wiesner et al. 2010). The representatives of this family of enzymes found to date in mammals are acetylcholinesterase (AChE) and butyrylcholinesterase (BChE). These enzymes differ from one another in both function and substrate selectivity terms. While AChE basically processes neurotransmitter acetylcholine (ACh) at cholinergic synapses and neuromuscular junctions, BChE is also able to process other substrates and is found in liver, heart, brain, and blood serum, but has no exact well understood function (Wiesner et al. 2010). It is believed that the differences in selectivity and specificity between these enzymes are related to the differences in their active site structures (Harel et al. 1992; Kovarik et al. 2003). The specificity observed for AChE was due to the shape of its active site, whose catalytic triad is located at the bottom of a narrow 20 Å deep gorge that does not allow the access of substrates larger than ACh. BChE, however, possesses a larger active site and spacious acyl pocket, and allows the access of substrates bigger than ACh, like butyrylcholine. About 50 residues are estimated to be implicated in the main cavity (Çokuğras 2003), while the following binding sites have been described in BChE (Çokuğras 2003; Suárez and Field 2005):

1. Peripheral anionic site (PAS) containing Asp70 and Tyr332 (Y332). Positive charged substrates form a cation-π complex with the aromatic ring of Tyr332, and interact with the negatively charged Asp70. This induces conformational changes transferred to the gorge at the active site.
2. Omega loop: Trp430, as well as Trp231 and Trp82, appear to form the wall of the active site gorge, whose dynamics seems to determine the transfer of the substrate to the active site.
3. Choline binding site, or cation-π site, containing Trp82 inside the gorge. The equivalent site in AChE was known before as the "anionic site", but in BChE, it is not "anionic", but depends on Trp82 and binds the Ch group through cation-π binding.
4. Oxyanion hole, near the cation-π-site, helps rotate the substrate containing Gly116, Gly117 and Ala199 to facilitate the approach of the acyl group of the substrate to the acyl binding site, and to layer the substrate at the catalytic site.
5. Acyl binding site, with aliphatic residues (Leu286 and Val288), and also Asp68 and Gln119, where there are aromatic residues in AChE. The smaller and more flexible side chain generates a wider gorge and allows the access of larger substrates in BChE. The hydrophobic binding of the acyl group prepares the substrate for hydrolysis. Binding and interacting to these residues have been suggested to explain mixed non-competitive inhibition of diterpenes (Wong et al. 2010).
6. Catalytic site, containing Ser198, Glu325, and His438 has been classically considered the "esteratic site" of the active center, in which the electron transfer from His438, facilitated by Glu325, allows Ser198 to make a nucleophilic attack and form the acyl-enzyme in the catalytic mechanism.
7. Other residues, such as Ser322, Glu325, His428, and the peptide linkage between Val321 and Asn322, have been reported to be important in the catalytic mechanism (Suárez and Field 2005; Suárez et al. 2006).

The interaction of ligands at sites other than the catalytic center, including the interaction from beyond the main cavity (gorge) or the interaction in the mouth of the gorge of the substrate, and other ligands on the aromatic ring of Tyr332, and on Asp70 of the PAS, might modulate conformational changes at the active site (Masson et al. 1999). Two substrate-binding loci, Asp70 in the PAS and Trp82 at the active site, are connected by the so-called Omega loop and implicate residues Glu197 and Ala328; they have been reported to be involved in substrate activation. This is interpreted as an allosteric effect at the active site due to the binding of the second substrate molecule to the PAS. The alterations related with the residues in the wall and omega loop (Trp430, Trp231 and Trp82) may induce conformational changes by determining the interaction of the substrate with the active site (Masson et al. 2001).

Interactions at the choline site or acyl pocket have been considered to interpret the non-competitive or non-competitive mixed-type inhibitions observed by diterpenes (Wong et al. 2010) as a kind of allosteric effect. However, this kinetic interpretation implies uncertainties because the substrate activation process is not considered in the kinetic mathematical model, which does not follow the simple Michaelis Menten kinetics. Nevertheless, no full explanation has yet been provided, and other residues and binding sites might be involved.

Therefore, besides the active site-related loci (choline and acyl binding sites), BChE also potentially possesses

further binding sites where other ligands can bind and/or be processed, which would affect the role of the choline or acyl binding sites, and the actual catalytic function by the catalytic triad and subsequent kinetic behavior.

Phenyl valerate (PV) was the substrate used to identify and characterize neuropathy target esterase (NTE) (Johnson 1975; Chemnitius et al. 1983; Carrington and Abou-Donia 1984; Vilanova et al. 1990; Glynn et al. 1994, 1998) and other serine hydrolases of neural tissue and brain (Céspedes et al. 1997; Escudero et al. 1997; Barril et al. 1999; Estévez et al. 2004, 2010, 2011).

In a soluble brain fraction of chicken, three enzymatic components have been discriminated using irreversible inhibitors as follows: mipafox (OPIDN-inducer), paraoxon (non OPIDN-inducer) and phenylmethylsulfonyl fluoride (PMSF) (Mangas et al. 2011, 2012).

Benabent et al. (2014) have shown that PV (the substrate of PVase activity) partially inhibits ChE activity in soluble brain fractions of chicken, and vice versa, while acetylthiocholine (AtCh) displays some inhibition in PVase activity components. This scenario suggests that PVase components may contain enzymes that hydrolyze ACh. Through a proteomic analysis, it has been demonstrated that a fraction enriched with the Eα component of PVase activity contains BChE (Mangas et al. 2017a).

Mangas et al. (2017b) have reported that purified hBChE also presents phenyl PV esterase activity, which corroborates lack of the substrate specificity of BChE, and demonstrates that a relationship between hBChE and PVase activities is also relevant for humans as is, therefore, the potential role in toxicity for humans.

Inhibition by the pre-incubation of PVase and the ChE activities of hBChE with irreversible inhibitors (mipafox, iso-OMPA or PMSF) demonstrates that these inhibitors interact similarly in both activities with comparable second-order inhibition constants. AtCh and PV partly inhibit PVase and ChE activities, respectively (Mangas et al. 2017b). All these observations suggest that both activities occur at the same active center. However, the kinetics of the interactions between substrates were not conclusive for the interpretations of the kinetics and the molecular interactions with the enzyme, particularly for the interpretation of the kinetic interactions between substrates.

To look at this issue in more depth, further studies have been done in this paper into two aspects: (a) the kinetic analysis of the enzymatic reactions with both substrates (AtCh and PV) and of the interactions between them; (b) the theoretical docking studies and molecular dynamic simulations were performed to search for insights as to the most likely binding pockets of PV.

Through docking algorithms (Thomsen and Christensen 2006; Trott and Olson 2010), it is possible to search for alternative pockets where PV can bind with energy values that are similar to or lower than it can be at the choline pocket. Further molecular dynamic simulations, followed by molecular mechanics Poisson–Boltzmann surface area (MM-PBSA) free energy calculations (Kumari et al. 2014), were used to check the stability of ligands at other potential binding sites.

The objective of this paper was to establish the kinetics of the interaction between substrates, and with theoretical research combined with experimental kinetic studies, to indicate the correct binding site of PV inside hBChE and to help properly interpret its enzymatic kinetics with substrates, as well as the kinetics of the interactions between substrates.

Materials and methods

Chemicals

Sodium dodecyl sulfate (SDS; purity 99%) was obtained from Panreac Química S.L.U. (Barcelona, Spain). Ellman's reagent, 5,5′-dithio-bis-2-nitrobenzoate (DTNB, purity 99%) and AtCh iodide (purity ≥ 98) were purchased from Sigma (Madrid, Spain). PV was attained from Lark Enterprise (Webster, MA, USA) and was checked in our laboratory by GC/MS, observing that it contains less than 0.1% phenol and less than 1% of other carboxylesters as impurities. All the other reagents were obtained from Merck SL (Madrid, Spain) and were of analytical grade.

Solutions

"Phosphate buffer", which is mentioned throughout, contained 0.1 M phosphate, pH 7.4, 1 mM EDTA.

A stock solution of substrate PV (150 mM) was prepared in dried *N,N*-diethylformamide,and was diluted in water at the concentrations indicated in each assay, immediately before the enzymatic assays. AtCh was prepared in water before being used at the concentrations indicated in each assay immediately before the enzymatic assays.

To stop the enzymatic reaction and color development, the following solutions were prepared: SDS-AAP solution (for PVase activity): a 2% SDS (sodium dodecyl sulfate) that contained 1.23 mM aminoantypirine in phosphate buffer. SDS-DTNB solution (for ChE activity): a 2% SDS solution that contained 6 mM DTNB in phosphate buffer.

Enzyme

Purified hBChE, isolated from human plasma, was a gift from Dr David Lenz and Dr Douglas Cerasoli [USAMRICD (US Army Medical Research Institute of Chemical Defense), Aberdeen Proving Ground, MD, U.S.A.]. All the enzyme

concentrations refer to the concentration of catalytic sites, i.e. monomers.

Measuring esterase activities

PVase and ChE activities were both inhibited and measured by a similar strategy and procedure to enable the comparison of the response to inhibitors and to evaluate the interaction between the substrates under comparable conditions. Enzyme preparation was pre-incubated with the inhibitor for the desired time (needed for the irreversible inhibitor), the substrate was added for a set time of 5.25 min and the reaction was stopped with a mixture that contained SDS, plus the color reagent (SDS-AAP or SDS-DTNB solutions for PVase or ChE, respectively).

An automated Work Station (Beckman Biomek 2000) was employed for the pipetting and incubating process with inhibitors and substrates.

PVase activity

PVase activity was measured according to Mangas et al. (2011) by following a procedure based on the colorimetric method for the NTE assay developed by Johnson (1977), and using an automated Work Station (Beckman Biomek 2000) for the full procedure as follows: 120 µl volume samples of the enzyme preparation 1 nM hBChE (buffer in blanks for spontaneous hydrolysis) were incubated with 120 µl of PV at the concentration indicated in each experiment. The mixture was incubated for 5 min and 25 s at 37 °C for the enzyme reaction with the substrate. The reaction was stopped by adding 120 µl of SDS-AAP solution after mixing. Next 60 µl of 1.21 mM potassium ferricyanide were added and left for 5 min for color development. A 300-µl volume from each microtube was transferred to a 96-well microplate. Absorbance was read at 510 nm in a microplate reader (Beckman Coluter AD 340). Blanks (samples without hBChE) were included for the spontaneous hydrolysis and the same procedure was applied.

ChE activity

Assays were carried out according to Benabent et al. (2014). First 120 µl volume samples of the enzyme preparation 1 nM hBChE (buffer in blanks) were incubated with 120 µl of AtCh in ultrapure water, at the concentration indicated in each experiment for 5 min and 25 s at 37 °C, to measure enzymatic activity. The enzymatic reaction was stopped by adding 120 µl of SDS-DTNB solution. Then 120 µl of phosphate buffer (the diluted enzyme preparation in the blanks) were added. The final assay volume was 480 µl. After mixing and waiting for at least 5 min, a 300 µl volume from each microtube was transferred to a 96-well microplate to read absorbance at 410 nm.

Mathematical models and kinetic data analysis

General approach

The results of the kinetic experiments were processed by version 13 of the SigmaPlot software (Systat Software Inc, Chicago, USA) for Windows®. Non linear regression was used with the Enzyme Kinetics Module to obtain the best fitting kinetic model and to calculate the kinetic parameters. The equations describing the kinetics for the substrate interactions (Hill, Michaelis–Menten, activation by substrate, inhibition by substrate, iso-enzyme and biphasic substrate activation) and the competitive (full and partial), uncompetitive (full and partial), non-competitive (full and partial) and mixed (full and partial) inhibitions, were used to fit the data sets. Other models, which consider one substrate to be the inhibitor of the other, were tested using the model included in the Sigma Plot software v13 (Systat Software Inc, Chicago, USA). More than 80 kinetic mathematical models were developed, including substrate activation with the different inhibition types, and they were also evaluated. The best fitting model was established by comparing the different models (Akaike 1974) and by selecting the best fitting one using the software facilities. This procedure has been extensively used in the literature (Li et al. 2004; Fišar et al. 2010; Calamini et al. 2010).

Model of substrate activation

This behavior of butyrylcholinesterases, with excess substrate that does not follow the Michaelis–Menten kinetics, is usually explained with the reaction model, as shown in Fig. 1 in Supplementary Material.

The reaction model, in which substrate molecule S binds to two different (active and peripheral) sites with two dissociation constants (K_m and K_{ss}), can be used to describe substrate activation at high substrate concentrations.

The substrate can be bound to either the free enzyme or the ES Michaelis complex (Fig. 1 in Supplementary Material). The mathematical model equation derived from this mechanism is shown in Eq. 1 where V_1 is the maximum rate of the non-activated enzyme and V_2 is the maximum rate of the activated enzyme by excess of substrate:

$$V = \frac{V_1 \cdot S + V_2 \cdot \frac{S^2}{K_{ss}}}{K_m + S + \frac{S^2}{K_{ss}}}. \quad (1)$$

Model of substrate competition

The data obtained in the substrate competition experiments were analyzed in a first tier by a nonlinear computerized method based on the least squares principle through the

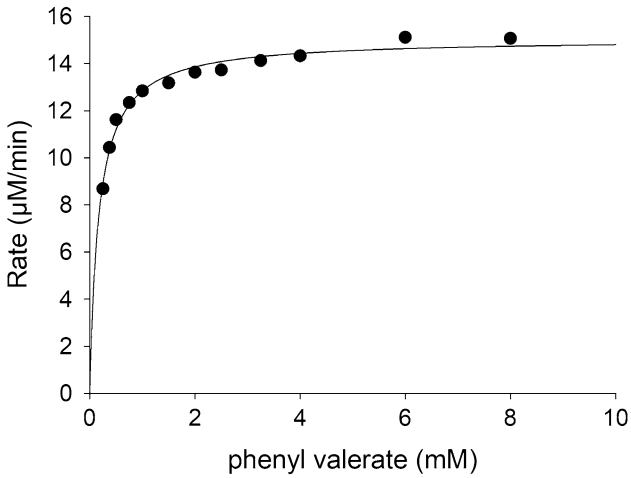

Fig. 1 The PVase activity of BChE. The line shows the best fit according to Akaike's criterion (Michaelis–Menten model; A Table 1)

SigmaPlot software, v13 (Systat Software Inc, Chicago, USA) for Windows®. The equation used to fit data was the equation deduced for two substrates, which compete in the same active center in two possible situations: (A) both substrate reactions are according to the Michaelis–Menten kinetics (Fig. 2 in Supplementary Material), whose mathematical model equation is shown in Eq. 2 (Cornish-Bowden 2004). (B) The alternative is a biphasic substrate activation reaction for one substrate, considering a Michaelis–Menten reaction for the other substrate (Fig. 3 in Supplementary Material, Eq. 3). V_1 is the maximum rate of the non-activated enzyme and V_2 is the maximum rate of the activated enzyme by excess of substrate:

$$V = \frac{V_{\max} \cdot S_1}{S_1 + (1 + \frac{S_2}{K_{m2}}) \cdot K_{m1}}, \tag{2}$$

$$V = \frac{V_1 + \frac{V_2 \cdot S}{K_{ss}}}{1 + \frac{K_m}{S} + \frac{K_m \cdot S'}{K_{m1} \cdot S} + \frac{K_m S'}{K_{m2} \cdot K_2} + \frac{K_m + S}{K_{ss}}}. \tag{3}$$

Models when a substrate is considered the inhibitor of the hydrolyzing activity of the other substrate

Several models included by default in the Enzyme Kinetic Module of the Sigma Plot (Systat Software Inc, Chicago, USA) were tested. The best fits were deduced according to Akaike's criterion. The partial mixed inhibition model (Eq. 4; Fig. 4 in Supplementary Material) was the best to fit to the experimental data of PV hydrolyzing activity in the presence of AtCh:

$$V = \frac{\left(V_{\max} + \frac{V_{\max} \cdot \beta \cdot I}{\alpha \cdot K_i}\right) \cdot S}{K_m \cdot \left(1 + \frac{I}{K_i}\right) + \left(1 + \frac{I}{\alpha \cdot K_i}\right) \cdot S}. \tag{4}$$

In another way, we deduced more than 80 different model equations of reversible inhibition to fit them to the experimental data of AtCh hydrolyzing activity in the presence of PV.

These model equations took into account that the AtCh hydrolyzing activity of hBChE is activated in the presence of substrate and, therefore, the different kinds of reversible inhibition (full and partial competitive, full and partial uncompetitive, full and partial non-competitive and full and partial mixed inhibitions) are considered in both the non-activated enzyme and the activated enzyme. All these models were evaluated by processing and analyzing the data by adapting the model equation with the Enzyme Kinetic Module of Sigma Plot (Systat Software Inc, Chicago, USA).

The best model fitted to our data (see the "Results") was a non-competitive inhibition when the enzyme was non activated and the partial non-competitive inhibition occurred when the enzyme was activated (Fig. 5 in Supplementary Material). Equation 5 describes the kinetic behavior:

$$V = \frac{V_1 + \frac{V_2 \cdot S}{K_{ss}} + \frac{V_3 \cdot S \cdot I}{K_{ss} \cdot K'}}{1 + \frac{K_m}{S} + \frac{K_m \cdot I}{K_i \cdot S} + \frac{(K_m + S) \cdot I}{K_i \cdot K_{ss}} + \frac{K_m + S}{K_{ss}} + \frac{I}{K'_i}}. \tag{5}$$

Docking studies

For the molecular docking studies, the Molegro Virtual Docker (MVD)® software was used. The crystallographic structure of hBChE complexed with Ch (Nicolet et al. 2003), obtained from the protein data bank (PDB) (Berman et al. 2000) under the code 1P0M, was used for this study. Co-crystallized molecules were removed and missing residues were added using the software SPDBViewer (Guex and Peitsch 1997; Schwede et al. 2003). Crystallographic water molecules were kept in order to investigate eventual interactions with the solvent, during the calculations. After structural optimizations, docking was performed on the larger hBChE cavity, which contains the aminoacids of the catalytic site, including the Ch binding site, the acyl binding site, the catalytic triad, and other residues. The employed protocol was validated through re-docking of Ch over its experimental structure from the crystal.

The dockings of PV and ACh were performed without considering the presence of Ch. Thus, the resulting configurations were those that interacted in the most energetically favorable regions.

We performed four runs in the docking studies, changing parameters of the algorithm and obtained 120 conformations for PV and 120 conformations for ACh. For the first simulation, the default docking algorithm of MVD® was used. For the others, the parameter population size was defined for 100, 150, and 200 initial conformations. Afterwards, conformations were grouped according to their energy, and the cavity regions where they interacted. The interaction energies were calculated according to the punctuation function (Eq. 6), which involved predicting binding energies (Azevedo et al. 2012; Huang and Zou 2010; Thomsen and Christensen 2006), the intermolecular interactions between the ligand and protein, and the intramolecular interactions of each ligand (Thomsen and Christensen 2006):

$$E_{\text{score}} = E_{\text{inter}} + E_{\text{intra}}, \tag{6}$$

where E_{inter} refers to the interaction energy between ligand and protein and was calculated as shown in Eq. 7:

$$E_{\text{inter}} = \sum_{i=\text{ligand}} \sum_{j=\text{protein}} \left[E_{\text{PLP}}\left(r_{ij}\right) + 332.0 \frac{q_i q_j}{4 r_{ij}} \right], \tag{7}$$

where the sum includes all the atoms of the ligand, the cofactor or water molecules, and the protein. The term E_{PLP} is the piecewise linear potential that uses parameters that come close to the steric term (van der Walls) between the atoms, and a potential to describe hydrogen bonds (H-bonds). The second term is the Coulomb potential, multiplied by 332.0 to convert the units of electrostatic energy into kcal mol^{-1} (Thomsen and Christensen 2006).

The term E_{intra} from Eq. 6 is described by Eq. 8.

$$E_{\text{intra}} = \sum_{i=\text{ligand}} \sum_{j=\text{protein}} E_{\text{PLP}}\left(r_{ij}\right) + \sum_{\text{flexible bonds}} A\left[1 - \cos\left(m\theta - \theta_0\right)\right] + E_{\text{clash}}, \tag{8}$$

where the first term describes all the pairs of atoms in the ligand, excluding the pairs not connected by two bonds or fewer. The second term refers to the torsional energy parameterized according to the kind of hybridization of the bonded atoms, where θ is the torsional bond angle. The term E_{clash} attributes a penalty of 1000 if the distance between 2 atoms, separated from one another by 2 bonds or more, is less than 2.0 Å (Thomsen and Christensen 2006).

Molecular dynamics simulations

From the docking study, two sites were selected to perform the molecular dynamic (MD) simulations: one in the "active site region" related to the catalytic active site, and the other region with the best favorable poses for PV. The best poses of ACh, Ch and PV inside hBChE, obtained from the docking studies, were parameterized to the force field OPLS-AA (Hu and Jiang 2009) with the ACPype software (Silva and Vranken 2012) and their atomic charges were calculated by the RESP method (Bayly et al. 1993; Cornell et al. 1993). Finally, the MD simulations were performed with the GROMACS 4.6.7 software (Hess et al. 2008; Van der Spoel et al. 2005) in the following systems:

- hBChE-ACh; hBChE-Ch; hBChE-PV (with Ach, Ch and PV bonded to the catalytic site);
- PV-hBChE (with PV bonded to the other PV best docking site region),
- PV-hBChE-ACh (with ACh bonded to the catalytic site and PV bonded to the other PV best docking site region),
- PV-hBChE-Ch (with Ch bonded to the catalytic site and PV bonded to the other PV best docking site region),
- ACh-hBChE-PV (with PV bonded to the catalytic site and ACh bonded to the other PV best docking site region),
- Ch-hBChE-PV (with PV bonded to the catalytic site and Ch bonded to the other PV best docking site region) and
- PV-hBChE-PV (with PV bonded to both regions).

Note that the nomenclature used is as follows: Y-hBChE-X, being X the ligand bound at the active site, and Y the ligand bonded to the PV best docking site, named as "PV-site".

In order to run the MD simulations, systems were confined inside octahedral boxes under periodic boundary conditions (Martínez et al. 2007). Each box was filled with TIP4P-type water molecules (Jorgensen et al. 1983) to reproduce the effect of the solvent. Afterwards, the energy minimization of each system was performed in four steps: (1) steepest descent algorithm with position restrained (PR), for better adjustment of water molecules; (2) steepest descent without PR, in both cases the convergence criterion was 100.00 kJ mol^{-1} nm^{-1}; (3) conjugate gradients (CG), with a convergence criterion of 20.00 kJ mol^{-1} nm^{-1}; (4) low-memory Broyden–Fletcher–Goldfarb–Shanno algorithm approach considering the minimization as converged when smaller than 1.00 kJ mol^{-1} nm^{-1}. Energy minimizations were followed by the thermalization steps, through the canonical ensemble (NVT) (Bosko et al. 2005), keeping constant the number of particles, volume and temperature, with a time of 100 ps, and the isothermal isobaric ensembles (NPT) (Bosko et al. 2005), to balance the pressure and temperature of the complexes, keeping constant the number of particles, pressure, and temperature. The minimized and equilibrated systems were also submitted to 500 ps of the MD simulations with PR for the enzyme and ligands to ensure a better accommodation of the water molecules around the amino acids of the enzyme. This was followed by a production step of 40 ns at 310 K and 1 bar, using 2 fs of integration time with the lists

of pairs being updated at every 5 steps. The cut-off for Lennard–Jones interactions were 0 between 0 and 1.2 nm and the cut-off for Coulomb interactions were 0 between 0 and 1.2 nm. The leap-frog algorithm was used in the production step with Nose–Hoover thermostat (Evans and Holian 1985) ($\tau = 0.5$ ps) at 298 K and the Parrinello–Rahman barostat (Parrinello and Rahman 1981) ($\tau = 2.0$ ps) at 1 bar. All Arg and Lys residues were assigned with positive charges and all residues Glu and Asp were assigned with negative charges. In order to analyze the behavior of the systems, the plots of the root-mean-square deviation (RMSD) and the average H-bonds formed during the simulation were drawn.

Binding energy calculations

The MM-PBSA method has been extensively used for free energy calculations (Almeida et al. 2015; Bastos et al. 2016; de Souza et al. 2016; Jayaram et al. 1998; Kar et al. 2013; Shao et al. 2006; Vorobjev et al. 1998). It uses the Poisson–Boltzmann equation (PB) to solve the contributions to the energy for binding a ligand to a protein. Despite overestimating the absolute binding free energy, MM-PBSA is considered a good method to calculate relative binding free energies in ligand–protein systems (Homeyer and Gohlke 2012; Kumari et al. 2014). In order to calculate the binding energies of the ligands in the complexes with hBChE, the g_mmpbsa software was used (Baker et al. 2001; Kumari et al. 2014). In the MM-PBSA method the binding free energy is defined as follows:

$$\Delta G_{\text{bind}} = \Delta G_{\text{complex}} - G_{\text{protein}} - G_{\text{ligand}}. \quad (9)$$

In our case, the free energy was calculated using Eq. 10:

$$\Delta G_{\text{bind}} = \Delta G_{\text{complex}} - (G_{\text{HssBChE}} + G_{\text{ligands}}), \quad (10)$$

where G_{complex} represents the free energy of the complexes (in our case hBChE-ACh, hBChE-Ch, hBChE-PV, PV-hBChE, PV-hBChE-ACh, PV-hBChE-Ch, ACh-hBChE -PV, Ch-hBChE -PV and PV-hBChE-PV), G_{hBChE} represents the free energy of the protein (hBChE in our case) and G_{ligands} (ACh, Ch, PV1, PV2, ACh + PV, Ch + PV and PV + PV) represents the free energy of the ligands.

Each term in Eq. 10 must be calculated in the following way:

$$G_{\text{term}} = \langle \text{EMM} \rangle - TS + \langle G_{\text{solvation}} \rangle, \quad (11)$$

where "< >" represents the mean values, G_{term} could be the complex protein-cofactor or protein–ligand (in our case), and EMM is the mechanical potential energy in vacuum. Temperature and entropy are depicted by terms T and S, respectively, which together represent the entropic contribution to the free energy in vacuum. The energy needed to transfer a solute from the vacuum to the solvent ($G_{\text{solvation}}$) is called the free energy of solvation and is obtained from the sum of two terms:

$$G_{\text{solvation}} = G_{\text{polar}} + G_{\text{nonpolar}}. \quad (12)$$

G_{polar} arises from the electrostatic interaction between the solute and the solvent and is obtained by solving the PB equation using the implicit (continuum) approach (Kumari et al. 2014).

In the PB equation, $\varphi\ (r)$ represents the electrostatic potential. For $\varphi\ (r) << kT$ (where k is the Boltzmann constant and T is temperature), $\sinh[\varphi(r)] \approx \varphi(r)$, and the PB equation become linear:

$$\nabla \cdot [(r)\nabla \cdot \varphi(r)] - \varepsilon(r)k^2(r)\sinh[\varphi(r)] + \frac{4\pi\rho(r)}{kT} = 0, \quad (13)$$

where ε is the dielectric constant, ρ is the fixed charge density, and k^2 is related to the reciprocal of the Debye length, which is dependent on the ionic strength of the solution.

Of the several models available for apolar calculation, we used the SASA model (Sitkoff et al. 1994) with a surface tension of 0.0226778 (kJ mol^{-2}) and a probe radius of 1.4 Å. For the calculations, dielectric constants of 6, 80 and 1 were used for the protein, water and void, respectively.

In order to consider non correlated frames, the structures for the free energy calculations were obtained at each 500 ps (a value higher than the correlation time) to ensure different energy states of the protein for each frame.

Results

Hydrolysis of PV by hBChE

The incubation of PV at concentrations within the 0.250–8.000 mM range with 1 nM hBChE hBChE 0.5 nM in reaction volume yielded a behavior of a rectangular hyperbola (Fig. 1) and activity up to ~ 15 µM min^{-1} (up to 8 mM PV). Data were analyzed for all the enzymatic models available in the Enzyme Kinetic Module of Sigma Plot software (Systat Software Inc, Chicago, USA). The best model fitted to the data according to Akaike's criterion was a classical Michaelis–Menten model in five independent experiments. Average values of Km, Vmax and kcat are given in Table 1 and the individual values of the kinetic parameters for each independent experiment are indicated in Supplementary Material Table 1.

Interaction of AtCh with PVase activity

Fitting with the competition model between PV and AtCh

PVase activity was assayed in the presence of 0.5, 3 and 20 mM of AtCh, and was tested for PV as a substrate at

Table 1 Mathematical model equation of some of the evaluated kinetic models

Experiment (n number of experiments)	Equation number (model)	Results Parameter ± SD (confidence interval 95%)
Hydrolysis of PV by hBChE ($n=5$, example in Fig. 1)	Michaelis–Menten	$K_m = 0.18 \pm 0.05$ (0.13–0.22) mM $V_{max} = 12.4 \pm 3.8$ (9.1–15.7) μM min^{-1} $k_{cat} = 24{,}960 \pm 7591$ (18,306–31,614) min^{-1}
Hydrolysis of AtCh by hBChE ($n=3$, xample in Fig. 3)	Equation 1 (Fig. 1 in Suppl. Material)	$K_{m1} = 0.06 \pm 0.02$ (0.04–0,09) mM $K_{ss} = 1.9 \pm 0.5$ (1.4–2.4) mM $V_1 = 15.3 \pm 2.0$ (13.1–17.5) μM min^{-1} $V_2 = 31.7 \pm 0.6$ (31.0– 32.3) μM min^{-1}
Interaction of AtCh with PVase activity ($n=5$, example in Fig. 2a) Fitting with the competition model between PV and AtCh	Equation 2 (Fig. 2 in Suppl. Material)	Equation 2 does not fit well to the experimental data
Interaction of PV with AtCh hydrolyzing activity ($n=3$, example in Fig. 3) Fitting with the competition model between PV and AtCh	Equation 3 (Fig. 3 in Suppl. Material)	Equation 3 does not fit well to the experimental data
Interaction of AtCh with PVase activity ($n=5$, example in Fig. 2b) AtCh as an inhibitor of PVase activity	Equation 4 (Fig. 4 in Suppl. Material)	$K_m = 0.20 \pm 0.06$ mM (0.15–0.25) mM $V_{max} = 12.6 \pm 3.9$ (9.2–16.0) μM min^{-1} $K_i = 0.39 \pm 0.13$ (0.27–0.51) mM $\alpha = 2.2 \pm 0.6$ (1.7–2.7) $\beta = 0.68 \pm 0.1$ (0.59–0.77)
Interaction of PV with AtCh hydrolyzing activity ($n=3$, example in Fig. 4) PV as an inhibitor of AtCh hydrolyzing activity	Equation 5 (Fig. 5 in Suppl. Material)	$K_m = 0.05 \pm 0.01$ (0.03–0.06) mM $K_{ss} = 1.5 \pm 0.3$ (1.1–1.9) mM $K_i = 1.4 \pm 0.6$ (0.7–2.0) mM $K_i' = 1.7 \pm 0.9$ (0.7–2.7) mM $V_1 = 14.0 \pm 0.8$ (13.1–14.8) μM min^{-1} $V_2 = 31.4 \pm 0.4$ (31.0–31.8) μM min^{-1} $V_3 = 17.6 \pm 4.1$ (13.0–22.3) μM min^{-1}

The reactions of the kinetic models are showed in Supplementary Material (Figs. 1–5). Equations 4 and 5 are models considering one substrate as inhibitor

the concentrations within the range from 0.25 to 8 Mm. Five independent experiments were performed.

In Fig. 2, panel A1 shows one example of the 3D fit to data (Estévez et al. 2004) with the mathematical equation deduced from the model of two substrates that competed for a same active site, according to the Michaelis–Menten kinetic reaction (Cornish-Bowden 2004; Fig. 2 in Supplementary Material; Eq. 2). The kinetic parameters are indicated in Table 2 model 1 in Supplementary Material for five independent experiments. Panel A2 of Fig. 2 shows the 2D curves related to the 3D surface shown in A1 at each of the tested AtCh concentrations. It is obvious that Eq. 2 does not fit well to the experimental data.

AtCh as an inhibitor of PVase activity

Panel B in Fig. 2 shows the best fit according to Akaike's criterion, obtained from processing the same data shown in panel A considering AtCh as an inhibitor. The result revealed that the best-fitting model was the mixed partial inhibition model in the five experiments (Eq. 4, indicated in "Materials and methods"). Average values of K_m, V_{max}, K_i, β and α are given in Table 1 and the individual values of the kinetic parameters for each independent experiment are indicated in Table 2, model 2 in Supplementary Material.

It is obvious that the models with equations that take AtCh as inhibitor fit better to the data than the model that considers classical competition between substrates.

Hydrolysis of AtCh by hBChE

The incubation of AtCh at the concentrations within the 0.250–10.000 mM range (with 1 nM hBChE 0.5 nM in a reaction volume) yielded a behavior of a hyperbola and activity up to ~ 30 μM min^{-1} (up to 10 mM AtCh). Figure 3 shows the best fit according to Akaike's criterion. The best-fitting model was the biphasic substrate activation model in three experiments (Eq. 1; with restriction $K_{ss} > K_m$). Average values of K_m, V_1, V_2 and K_{ss} are given in Table 1 and the individual values of the kinetic parameters for each independent experiment are indicated in Table 3 in Supplementary Material.

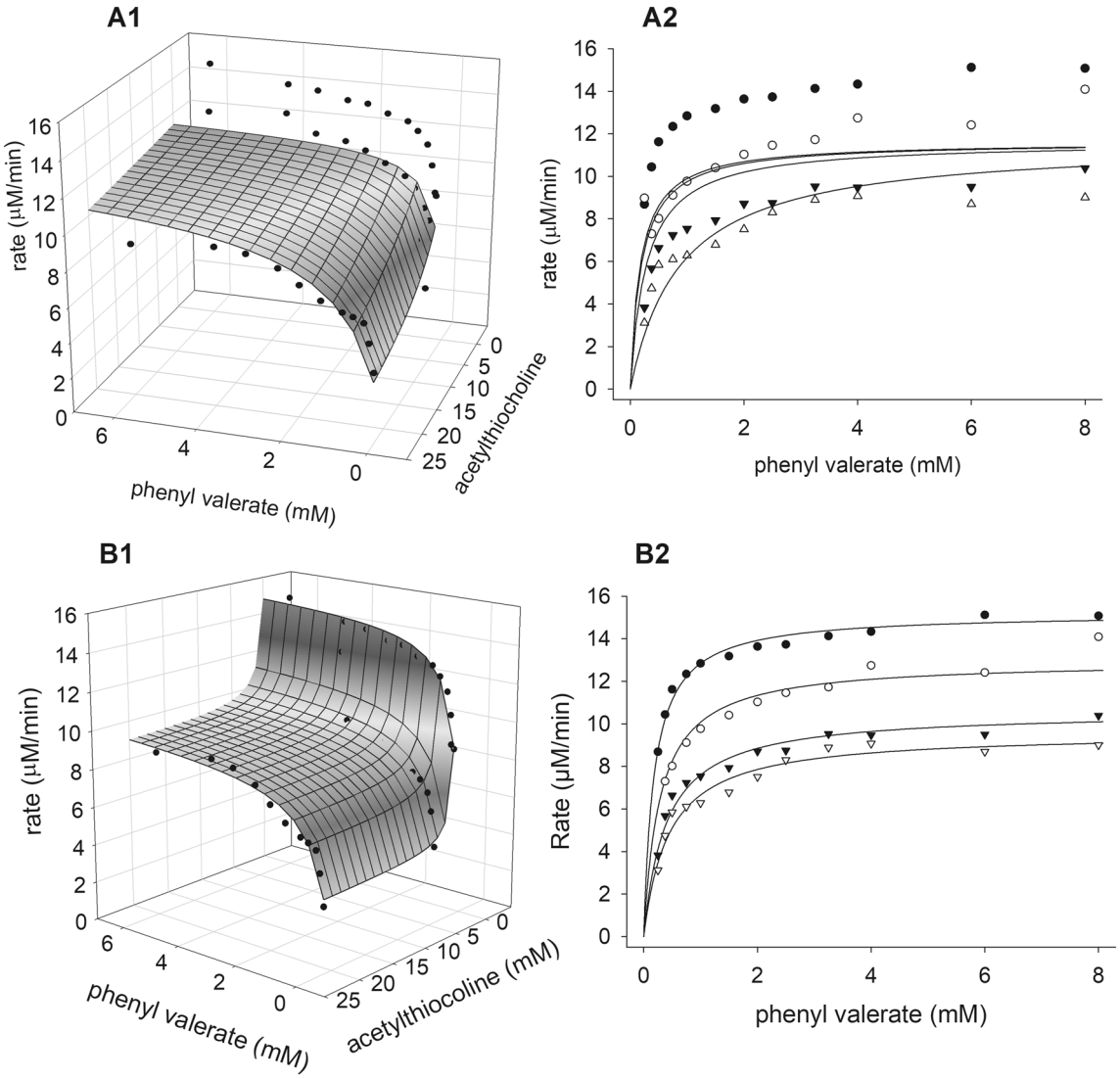

Fig. 2 PVase activity of hBChE in the presence of AtCh. One example of the three performed independent experiments is shown. PV concentrations (substrate): 0.25, 0.37, 0.50, 0.75, 1, 2, 2.5, 3.25, 4, 6 and 8 mM in. Inhibitor concentrations (AtCh): 0 (black circles), 0.5 (white circles), 3.0 (black triangles) and 20 mM (white triangles). **A** panels: Fitting the competition reaction model between two substrates with kinetic behavior according to the Michaelis–Menten reaction (Fig. 2 in Supplementary Material, Eq. 2; Table 1). **B** panels: Fitting when taking AtCh as an inhibitor. The fit corresponds to the partial mixed inhibition model (Eq. 4, Fig. 4 in Supplementary Material; Table 1). **A1** and **B1** show the 3D fit, while **A2** and **B2** show the level lines obtained from the 3D fit

Interaction of PV with AtCh hydrolyzing activity

Fitting with the competition model between PV and AtCh

AtCh hydrolyzing activity was tested in the presence of 0.5, 3 and 8 mM of PV and a 3D fit to data with the mathematical equation deduced from the model of two substrates that competed for a same active site, according to the biphasic substrate activation and the Michaelis–Menten kinetic reactions (Eq. 3, Fig. 3 in Supplementary Material). The estimated kinetic parameters are indicated in Table 4 in Supplementary Material for the three experiments. Panel A in Fig. 4 shows that Eq. 3 does not fit well to the experimental data. Panel A2 of Fig. 4 shows the level curves obtained from the surface shown in A1 at the PV concentrations used. Therefore, the competition model between substrates should be ruled out.

PV as an inhibitor of AtCh hydrolyzing activity

We deduced more than 80 different model equations of reversible inhibition to fit them to the experimental data

of AtCh hydrolyzing activity in the presence of PV. These model equations considered that the AtCh hydrolyzing activity of hBChE is activated in the presence of a substrate and, therefore, the different kinds of reversible inhibition (full and partial competitive, full and partial uncompetitive, full and partial non-competitive and full and partial mixed inhibitions) are contemplated in both the non-activated enzyme and the activated enzyme. All these models were evaluated by processing and analyzing data by adapting the model equation with the Enzyme Kinetic Module of the Sigma Plot (Systat Software Inc, Chicago, USA).

Of them all, the best-fitting model according to Akaike's criterion in three experiments was the model which included the non-competitive inhibition when the enzyme was not activated and the partial non-competitive inhibition when the enzyme was activated. The model is shown in the "Materials and Methods" (Fig. 5 in Supplementary Material, Eq. 5), and Panel B in Fig. 4 provides the results. Average values of K_m, K_{ss}, K_i, K_i', V_1, V_2 and V_3 are given in Table 1 and the individual values of the kinetic parameters for each independent experiment are indicated in Table 5 in Supplementary Material.

Docking studies

The energy obtained in the re-docking of Ch inside its crystallographic structure was −65.52 kcal mol^{-1}, with an RMSD of 0.86 Å. Considering that the literature reports RMSD values below 2.00 Å as being acceptable (Kontoyanni et al. 2004), our results validate the employed docking protocol. The overlapping of Ch and its crystallographic structure inside hBChE, and the interactions observed, are shown in Fig. 5.

Table 2 shows the interaction and H-bond energies and the interacting residues for the poses of each ligand selected from the docking studies. The dockings of PV afforded 120 energetically favorable poses, of which 95% interacted in the same pocket far from the catalytic site of hBChE (Fig. 6). Binding to this site involves an interaction with the residue Asn289, which we named the "PV-site". The other 5% favorable poses were in the catalytic pocket and interacted with Ser198 of the catalytic triad. For this reason, we selected the best poses of PV at each site to run the MD simulations. We also observed that Ch and PV formed H-bonds with His438 and Ser198 of the catalytic site.

Table 2 The docking results for the studied systems with hBChE

Ligand	MolDock Score (kcal mol^{-1})	H-bond (kcal mol^{-1})	Interacting amino-acids
ACh	−73.02	0.00	–
Ch	−56.34	−2.50	His438
PV (catalytic site)	−65.92	−2.13	Ser198
PV best docking site (PV-site)	−61.99	−1.52	Asn289

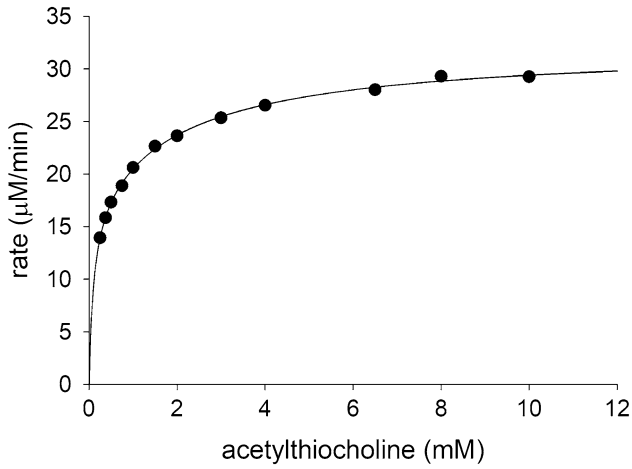

Fig. 3 ChE activity of hBChE with AtCh as a substrate. The line shows the best fit according to Akaike's criterion: the biphasic substrate activation model of the mechanism of biphasic substrate activation according to Eq. 1, Fig. 1 in Supplementary Material (Table 1)

Table 3 The MM-PBSA average free binding energies calculated between ligands and hBChE

Complex	Ligand (site)	Free binding energies (kcal mol^{-1})
hBChE-Ach	Ach (catalytic site)	−60.73
hBChE-Ch	Ch (catalytic site)	−66.58
hBChE-PV	PV (catalytic site)	−19.91
	PV (PV-site)	−26.96
PV-hBChE-Ach	Ach (catalytic site)	−69.93
	PV (PV-site)	−27.06
PV-hBChE-Ch	Ch (catalytic site)	−72.01
	PV (PV-site)	−38.12
ACh-hBChE-PV	PV (catalytic site)	−23.96
	ACh (PV-site)	−74.24
Ch-hBChE-PV	PV (catalytic site)	−26.93
	Ch (PV-site)	−80.28
PV-hBChE-PV	PV (catalytic)	−17.08
	PV (PV-site)	−30.48

MD simulations and binding energy calculations

The stabilities of the systems hBChE-ACh; hBChE-Ch; hBChE-PV;PV-hBChE, PV-hBChE-ACh and PV-hBChE-Ch were accessed from the RMSD plots (Fig. 6 in Supplementary Material), where we can see the position variation of molecules during the simulation time. Figure 7 in

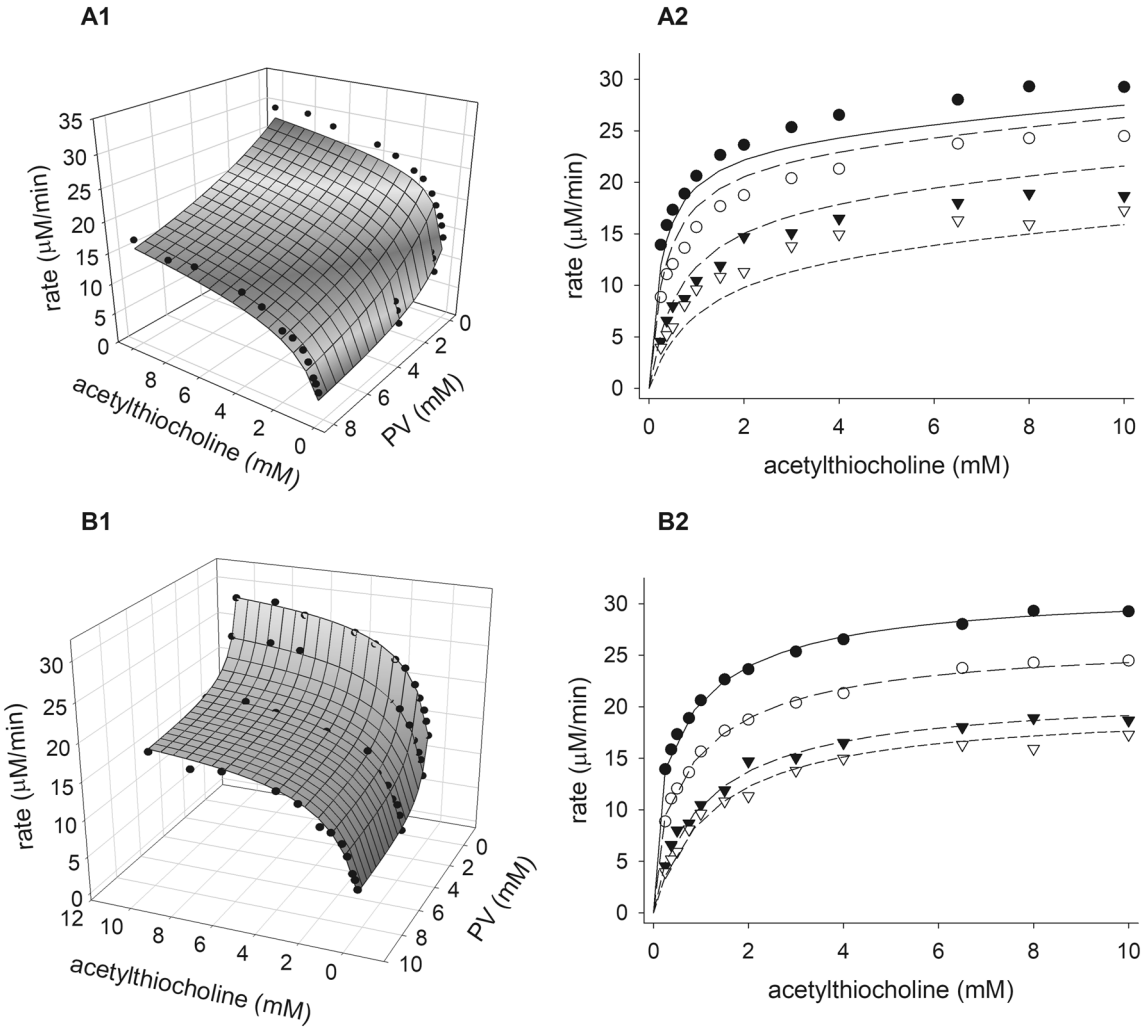

Fig. 4 ChE activity of hBChE in the presence of PV. One example of the three performed independent experiments is shown. AtCh concentrations (substrate): 0.25, 0.375, 0.5, 0.75, 1, 2, 3, 4, 6.5, 8 and 10 mM in 240 µl of the enzyme-substrate reaction volume. Inhibitor concentrations (PV): 0 (black circles), 0.5 (white circles), 3.0 (black triangles) and 8 mM (white triangles) in 240 µl of the enzyme-substrate reaction volume. **A** panels: The substrate competition model according to the model equation described in Fig. 3 in Supplementary Material, Eq. 3 (Table 1). **B** panels: The non-competitive inhibition model when the enzyme is not activated and the partial non-competitive inhibition when the enzyme is activated, according to the model indicated in Fig. 5 in Supplementary Material, Eq. 5 (Table 1). **A1, B1** Show the 3D fit and **A2, B2** indicate the level lines obtained from the 3D fit

Supplementary Material illustrates the variations in the center of mass (COM) distances between Ch and Ser198 during the MD simulation for complexes hBChE-Ch and PV-hBChE-Ch, while Fig. 7 shows the positions of PV, Ch and Ser198 inside hBChE after the MMPBSA calculations. The RMSD plots of complexes ACh-hBChE-PV, Ch-hBChE-PV, and PV-hBChE-PV are shown in Fig. 8 in Supplementary Material while Fig. 9 in Supplementary Material presents the COM variations among Ser198 and ACh, Ch, and PV for these systems. The MM-PBSA average free binding energies calculated between the ligands and hBChE are shown in Table 3.

Discussion

Hydrolysis of PV by hBChE

Mangas et al. (2017b) described PVase activity in hBChE. The data from this work confirm that the behavior of this activity is compatible with the Michaelis–Menten. The K_m and k_{cat} constants estimated in this work are comparable to the Km and k_{cat} estimated by Mangas and coworkers (K_m = 0.52/0.72 mM and k_{cat} = 45,900/49,200 min^{-1}).

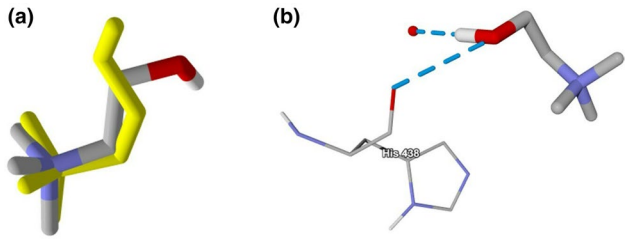

Fig. 5 Ch (CPK) overlapping its crystallographic structure (yellow) (**a**); interactions of the best Ch pose from the re-docking inside hBChE (**b**). (Color figure online)

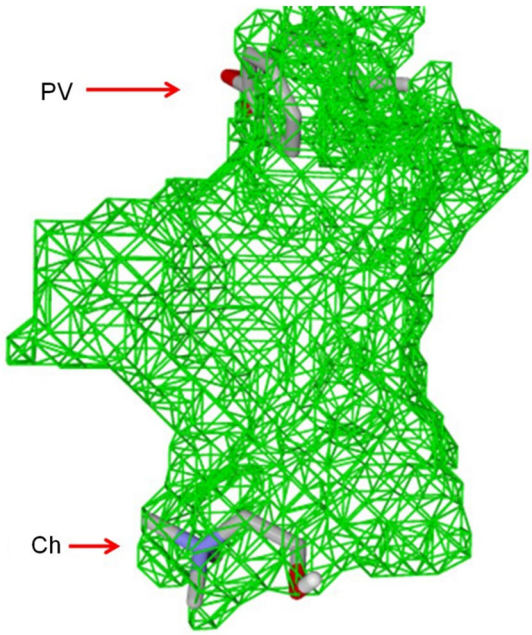

Fig. 6 Main binding pockets, oberved in the docking studies, for Ch and PV in the cavity of hBChE (shown in green). (Color figure online)

Interaction of AtCh with PVase activity

The results of testing PVase in the presence of AtCh show that PV and AtCh do not compete in a classical model of competition between substrates (Fig. 2a). In fact, if we consider AtCh as an inhibitor (Fig. 2b; Table 2 in Supplementary Material), the results suggest that AtCh interacts with PVase activity similarly to a reversible partial mixed inhibition (Fig. 4 in Supplementary Material). This kind of reversible inhibition is produced when the inhibitor interacts at sites other than the active site. According to the results of this work, AtCh partially inhibits PVase activity by interacting at different sites to the PV active site, while AtCh is hydrolyzed at the same time.

Hydrolysis of AtCh by hBChE

The results in Fig. 3 reveal that the model which best fit the AtCh hydrolyzing activity data is the biphasic substrate activation model (Eq. 1; with restriction $K_{ss} > K_m$). The estimated kinetic parameters are similar to those estimated by Masson et al. (1993) ($K_m = 0.049$ mM, $K_{ss} = 0.49$ mM) for this kinetic model. The experiment of AtCh hydrolyzing activity in the presence of PV shows that the model of competition between substrates (Fig. 4a) by the same active site does not fit well to the experimental data. In fact, if we consider PV as an inhibitor, the kinetics of the AtCh hydrolyzing activity in the presence of PV is compatible with the non-competitive inhibition by PV when the enzyme is not activated, and with the partial non-competitive inhibition when the enzyme is activated (Fig. 4b, Table 6 in Supplementary Material). This kind of reversible inhibition is produced when the inhibitor interacts at a different site to the active site when the enzyme is not activated, and when the enzyme is activated by excess of substrate.

The kinetic analysis suggests that PV partially inhibits the AtCh hydrolyzing activity by interacting at a different site to the AtCh active site.

Other considerations related to PV–AtCh interactions in hBChE

The partial inhibitions observed in the experiments of interactions between substrates shows that hBChE is able to hydrolyze both substrates simultaneously, independently of the substrate concentrations. The inhibition of PVase activity by AtCh is partial at high AtCh concentration, and vice versa, the activated ChE activity is inhibited partially. However, the non-activated hBChE is totally inhibited at high PV concentrations. These kinetic behaviors indicate a partial competition between both substrates allowing hBChE to hydrolyze both substrates at high concentrations. Others substrates (including biological substrates) could interact in similar way, giving the property to hBChE to be effective hydrolyzing more than one substrate simultaneously and increasing its property as scavenger.

Docking studies

From the docking studies, two binding sites are deduced for PV inside the active site cavity: one in the catalytic site region with the interaction with Ser198 (and His 438) of the catalytic triad, while the other is a favorable binding site situated far from the catalytic triad in which PV interacts with the Asn289 residue. We named this new site the "PV-site".

In Table 2 we can see that the obtained MolDock Scores (interactions enzyme-ligand) were similar for all the ligands,

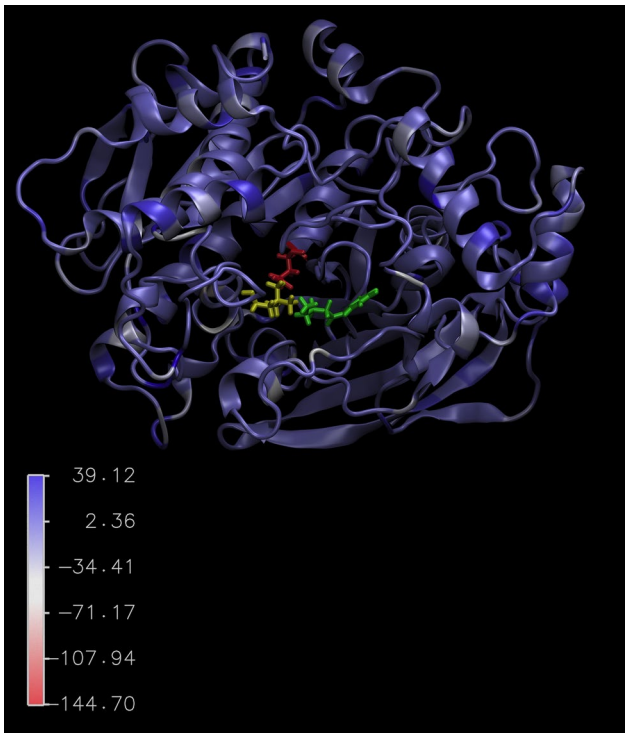

Fig. 7 The positions of PV (green), Ch (yellow) and Ser198 (red) inside the cavity of hBChE after 40 ns of MD simulations. (Color figure online)

and even PV gave similar values at both the allosteric PV-site and the catalytic site pockets. We also observed that Ch and PV formed H-bonds with Ser198 and His438, both of which are important residues of the catalytic site of hBChE.

MD simulations

Figure 6d in Supplementary Material shows that the complex PV-hBChE-Ch is the most stable with the narrowest variation in RMSD, while ACh presents a significant variation for RMSD (RMSDMáx.–RMSDMín.) between complexes hBChE-ACh (Fig. 6a in Supplementary Material) and PV-hBChE-ACh (Fig. 6b in Supplementary Material). In complex hBChE–Ch, Ch displays unstable behavior with wider RMSD variation (between 0.05 and 0.15 nm) (Fig. 6c in Supplementary Material), while this value remains stable, at around 0.10 nm, for the whole simulation time in complex PV–hBChE–Ch (Fig. 6d in Supplementary Material). Complexes hBChE–PV–1 and hBChE–PV–2, with PV docked at the active site and the PV-site, respectively (Figs. 9 in the text and 6f in Supplementary Material), present similar behavior to the PV RMSD variation, at around 0.12 nm in both cases. In comparison, PV behavior in complex hBChE–PV–Ch, is more stable, which suggests greater stability for PV inside hBChE when Ch is present.

Binding energies

The behaviors observed during the MD simulations, analyzed by the RMSD variations, suggest that PV influences the interactions of ACh and Ch with the active site of hBChE. The calculations of the average free binding energies of the complexes (Table 3) indicate that despite provoking wider RMSD variation of ACh and Ch, PV contributes to increase the stability of both ligands if the values obtained for the free binding energies of ACh in complex hBChE–PV–ACh and of Ch in complex PV–hBChE–Ch are more negative than the values obtained for these ligands in complexes hBChE–ACh and hBChE–Ch, respectively.

Our results of the average free binding energy for complex PV–hBChE (PV bound to the PV-site) (Table 3) suggest that PV shows no good potential for competitive inhibition. However, the binding free energy for PV at the PV-site presents a more negative value, which means a higher potential for non-competitive inhibition. Between complexes PV–hBChE–ACh and PV–hBChE–Ch, PV displays greater stabilization in complex PV–hBChE–Ch.

The narrowest RMSD variation and the values of free binding energies suggest that PV can inhibit the hydrolysis of ACh through interactions with the PV-site by avoiding the reaction or releasing Ch from the catalytic site. To check the influence of PV on the Ch interactions with the catalytic site, we also plotted the variation of distance between the COM of Ch and Ser198 during the MD simulations. As we can see in Fig. 7 in Supplementary Material, for complex hBChE–Ch this distance stabilizes only at about 25 ns of simulation at around 1 nm, while stabilization occurs after 10 ns at 0.63 nm, for complex PV–hBChE–Ch. This suggests that PV confers good stability to Ch at the active site, and the position occupied by PV in the cavity may avoid Ch from being released, as shown in Fig. 7.

The average free binding energies of the complexes with the PV docked at the catalytic site were calculated in order to check how the presence of PV at this site would influence the interactions of ACh, Ch and another PV molecule at the allosteric PV-site. The average energies of ACh and Ch at the PV-site (Table 3) showed an increase compared to the catalytic site. However, when analyzing RMSD during the simulated time (Figs. 8a and 8b hBChE in Supplementary Material) and the COM distances of ACh and Ch related to Ser198 (Figs. 9a and 9b in Supplementary Material), we observed that ACh presented a variation in position during simulation, which was directed towards the catalytic site, as shown by the shortening of its COM distance towards Ser198, and being stopped only by the presence of PV at the catalytic site. This suggests that PV is able to promote the competitive inhibition of hBChE to, thus, avoid ACh hydrolysis.

Figure 8b in Supplementary Material shows that Ch also changes position during MD simulation, but this time towards the opposite direction related to Ser198, as we can see from the COM distances shown in Fig. 9b in Supplementary Material. This suggests that the presence of PV at the catalytic site compromises the interactions with the Ch molecules.

The average free binding energies for the PV molecules inside complex PV–hBChE–PV, compared to complexes hBChE–PV (catalytic site) and PV–hBChE (PV-site), indicate a less intense interaction with the catalytic site and an increase in the interactions with the PV-site. The PV molecule at the PV-site lay in a more favorable position (see the free average binding energies of PV in this region for the complexes). This brings about a change in the enzyme conformation in this region that compromises the PV interactions at the catalytic site. This is seen in the plot of the RMSD and COM related to Ser198 (Figs. 8c and 9c in Supplementary Material), which reveals no variation during the simulated time. In the complexes where ACh and Ch are present at the catalytic site, this does not occur due to the better interactions of these molecules in this region.

Global remarks and conclusions

PV and AtCh are hydrolyzed at the same time. The results show that the interaction between both substrates is not compatible to a simple competition model between the substrates at the same active site. The interactions of PV in AtCh hydrolyzing activity, and vice versa, do not totally inhibit both activities, and these inhibitions are not a competitive reversible inhibition at the same active site. Therefore, the competition between these two substrates is not total; it is a partial competition and it can be directed thorough the interaction in other site different to the active site. After taking into account all the results as a whole, we conclude that the interactions between both substrates in hBChE are compatible with the interaction of two different sites for each substrate; indeed the inhibition of one substrate on the other activity is at least partly caused by the interaction at a different site to the active catalytic site through allosteric effects. Our docking studies and molecular dynamic simulations describe how it is compatible with interactions at a site related with residue Asn298, which is far from the catalytic site. We named it "PV-site" as the best energetically favorable poses are related with this site in the theoretical docking studies. As this is far from the catalytic site, the effect on catalysis by binding a ligand to this site (i.e.; a second molecule of the same substrate or another substrate, or another substance) would be considered an allosteric modulation. Further research is needed to understand the partial inhibition and the apparent absence of a total competitive interaction in the catalytic site. This will help to understand the role in the kinetics with substrates, inhibitors and the catalytic process in toxicity, as well as its role in the detoxication of xenobiotics.

Acknowledgements We are most grateful to Dr. Douglas Cerasoli [USAMRICD (US Army Medical Research Institute of Chemical Defense), Aberdeen Proving Ground, MD, USA] for the supply of hBChE.

Funding Work was partly supported by project "Mecanismos moleculares de toxicidad de xenobióticos" from the University Miguel Hernández of Elche (Spain), (Reference; 50AV0050RP). This work was supported by the Brazilian financial agencies CAPES (fellowships), CNPq (Grant No 306156/2015-6), FAPERJ (Grant No E-02/202.961/2017), and also the by the excellence project FIM.

References

Akaike H (1974) A new look at the statistical model identification. IEEE Trans Autom Control 19:716–723

Almeida JS, Guizado TR, Guimaraes AP, Ramalho TC, Goncalves AS, de Koning MC, Franca TC (2015) Docking and molecular dynamics studies of peripheral site ligand-oximes as reactivators of sarin-inhibited human acetylcholinesterase. J Biomol Struct Dyn 34:2632–2642

Azevedo LS, Moraes FP, Xavier MM, Pantoja EO, Villavicencio B, Finck JA, Proenca AM, Rocha KB, de Azevedo WF (2012) Recent progress of molecular docking simulations applied to development of drugs. Curr Bioinform 7(4):352–365

Baker NA, Sept D, Joseph S, Holst MJ, McCammon JA (2001) Electrostatics of nanosystems: application to microtubules and the ribosome. PNAS 98(18):10037–10041

Barril J, Estévez J, Escudero MA, Céspedes MV, Níguez N, Sogorb MA, Monroy A, Vilanova E (1999) Peripheral nerve soluble esterases are spontaneously reactivated after inhibition by paraoxon: implications for a new definition of neuropathy target esterase. Chem Biol Interact 119–120:541–550

Bastos L, da C, de Souza, Guimarães FR, Sirouspour AP, Guizado M, Forgione TRC, Ramalho P, França TC TCC (2016) Virtual screening, docking and dynamics of potential new inhibitors of dihydrofolate reductase from Yersinia pestis. J Biomol Struct Dyn 34:2184–2198

Bayly CI, Cieplak P, Cornell W, Kollman PA (1993) A well- behaved electrostatic potential based method using charge restraints for deriving atomic charges: the RESP model. J Phys Chem 97:10269–10280

Benabent M, Vilanova E, Sogorb MA, Estévez J (2014) Cholinesterase assay by an efficient fixed time endpoint method. MethodsX 1:258–263

Berman HM, Westbrook J, Feng Z, Gilliland G, Bhat TN, Weissig H, Shindyalov IN, Bourne PE (2000) The protein data bank. Nucleic Acids Res 28:235–242

Bosko JT, Todd BD, Sadus RJ (2005) Molecular simulation of dendrimers and their mixtures under shear: comparison of isothermal-isobaric (NpT) and isothermal-isochoric (NVT) ensemble systems. J Chem Phys 123(3):34905

Calamini B, Ratia K, Malkowski MG, Cuendet M, Pezuto JM, Santarsiero BD, Mesecar AD (2010) Pleiotropic mechanisms facilitated by resveratrol and its metabolites. Biochem J 429:273–282

Carrington CD, Abou-Donia MB (1984) The correlation between the recovery rate of neurotoxic esterase activity and sensitivity to

organophosphorus-induced delayed neurotoxicity. Toxicol Appl Pharmacol 75(2):350–357

Céspedes MV, Escudero MA, Barril J, Sogorb MA, Vicedo JL, Vilanova E (1997) Discrimination of carboxylesterases of chicken neural tissue by inhibition with a neuropathic, non-neuropathic organophosphorus compounds and neuropathy promoter. Chem Biol Interact 106(3):191–200

Chemnitius JM, Haselmeyer KH, Zech R (1983) Neurotoxic esterase. Identification of two isoenzymes in hen brain. Arch Toxicol 53(3):235–244

Çokuğraş AN (2003) Butyrylcholinesterase: structure and physiological importance. Turk J Biochem 28(2):54–61

Cornell WD, Cieplak P, Bayly CI, Kollman PA (1993) Application of RESP charges to calculate conformational energies, hydrogen bond energies, and free energies of solvation. J Am Chem Soc 115:9620–9631

Cornish-Bowden A (2004) In principles of enzyme kinetics, 3rd edn. In: Cornish-Bowden A (ed) Portland Press, London, pp 36–39

de Souza FR, Guimarães AP, Cuya T, de Freitas MP, Gonçalves AS, Forgione P, França TC (2016) Analysis of *Coxiela burnetti* dihydrofolate reductase via in silico docking with inhibitors and molecular dynamics simulation. J Biomol Struct Dyn 1102:1–12

Escudero MA, Céspedes MV, Vilanova E (1997) Chromatographic discrimination of soluble neuropathy target esterase isoenzymes and related phenyl valerate esterases from chicken brain, spinal cord, and sciatic nerve. J Neurochem 68(5):2170–2176

Estévez J, García-Perez A, Barril J, Pellín MC, Vilanova E (2004) The inhibition of the high sensitive peripheral nerve soluble esterases by mipafox. A new mathematical processing for the kinetics of inhibition of esterases by organophosphorus compounds. Toxicol Lett 151:243–249

Estévez J, Barril J, Vilanova E (2010) Inhibition with spontaneous reactivation and the "ongoing inhibition" effect of esterases by biotinylated organophosphorus compounds: S9B as a model. Chem Biol Interact 187(1–3):397–402

Estévez J, García-Pérez A, Barril J, Vilanova E (2011) Inhibition with spontaneous reactivation of carboxyl esterases by organophosphorus compounds: paraoxon as a model. Chem Res Toxicol 24(1):135–143

Evans DJ, Holian BL (1985) The Nose-Hoover thermostat. J Chem Phys 83(8):4069–4074

Fišar Z, Hroudová J, Raboch J (2010) Inhibition of monoamine oxidase activity by antidepressants and moodstabilizers. Neuro Endocrinol Lett 31(5):645–656

Glynn P, Read DJ, Guo R, Wylie S, Johnson MK (1994) Synthesis and characterization of a biotinylated organophosphorus ester for detection and affinity purification of a brain serine esterase: neuropathy target esterase. Biochem J 301(2):551–556

Glynn P, Holton JL, Nolan CC, Read DJ, Brown L, Hubbard A, Cavanagh JB (1998) Neuropathy target esterase: immunolocalization to neuronal cell bodies and axons. Neuroscience 83(1):295–302

Guex N, Peitsch MC (1997) SWISS-MODEL and the Swiss-PdbViewer: an environment for comparative protein modeling. Electrophoresis 18:2714–2723

Harel M, Sussman JL, Krejci E, Bon S, Chanal P, Massoulié J, Silman I (1992) Conversion of acetylcholinesterase to butyrylcholinesterase: modeling and mutagenesis. Proc Natl Acad Sci USA 89:10827–10831

Hess B, Kutzner C, Van der Spoel D, Lindahl E (2008) GROMACS 4: algorithms for highly efficient, load-balanced, and scalable molecular simulation. J Chem Theory Comput 4:435–447

Homeyer N, Gohlke H (2012) Free energy calculations by the molecular mechanics poisson-boltzmann surface area method. Mol Inform 31(2):114–122

Hu Z, Jiang J (2009) Assessment of biomolecular force fields for molecular dynamics simulations in a protein crystal. J Comput Chem 31:371–380

Huang SY, Zou X (2010) Advances and challenges in protein-ligand docking. Int J Mol Sci 11:3016–3034

Jayaram B, Sprous D, Young MA, Beveridge DL (1998) Free energy analysis of the conformational preferences of A and B forms of DNA in solution. J Am Chem Soc 120(41):10629–10633

Johnson MK (1975) Structure-activity relationships for substrates and inhibitors of hen brain neurotoxic esterase. Biochem Pharmacol 24(7):797–805

Johnson MK (1977) Improved assay of neurotoxic esterase for screening organophosphates for delayed neurotoxicity potential. Arch Toxicol 37(2):113–115

Jorgensen WL, Chandrasekhar J, Madura JD, Impey RW, Klein ML (1983) Comparison of simple potential functions for simulating liquid water. J Chem Phys 79:926–935

Kar P, Lipowsky R, Knecht V (2013) Importance of polar solvation and configurational entropy for design of antiretroviral drugs targeting HIV-1 protease. J Phys Chem B 117(19):5793–5805

Kontoyanni M, McClellan LM, Sokol GS (2004) Evaluation of docking performance: comparative data on docking algorithms. J Med Chem 47:558–565

Kovarik Z, Radić Z, Berman HA, Simeon-Rudolf V, Reiner E, Taylor P (2003) Acetylcholinesterase active centre and gorge conformations analysed by combinatorial mutations and enantiomeric phosphonates. Biochem J 373:33–40

Kumari R, Kumar R, Open Source Drug Discovery Consortium, Lynn A (2014) *g_mmpbsa*—A GROMACS tool for high-throughput MM-PBSA calculations. J Chem Inf Model 54(7):1951–1962

Li XQ, Andersson TB, Ahlström M, Weidolf L (2004) Comparison of inhibitory effects of the proton pump-inhibiting drugs omeprazole, esomeprazole, lanso-prazole, pantoprazole and rabeprazole on human cytochrome P450 activities. Drug Metab Dispos 32:821–827

Mangas I, Vilanova E, Estévez J (2011) Kinetics of the inhibitory interaction of organophosphorus neuropathy inducers and non-inducers in soluble esterases in the avian nervous system. Toxicol Appl Pharmacol 256:360–368

Mangas I, Vilanova E, Estévez J (2012) Phenylmethylsulfonyl fluoride, a potentiator of neuropathy, alters the interaction of organophosphorus compounds with soluble brain esterases. Chem Res Toxicol 25(11):2393–2401

Mangas I, Radić Z, Taylor P, Ghassemian M, Candela H, Vilanova E, Estévez J (2017a) Butyrylcholinesterase identification in a phenylvalerate esterase-enriched fraction sensitive to low mipafox concentrations in chicken brain. Arch Toxicol 91(2):909–919

Mangas I, Vilanova E, Estévez J (2017b) Phenyl valerate esterase activity of human butyrylcholinesterase. Arch Toxicol 91:3295–3305

Martínez L, Borin IA, Skaf MS (2007) Fundamentos de Simulação por Dinâmica Molecular. In: Morgon NH, Coutinho K (eds) Métodos de Química Teórica e Modelagem Molecular. Editora Livraria da Física, São Paulo, pp 413–452 **(ISBN: 9788588325876$4)**

Masson P, Adkins S, Gouet P, Lockridge O (1993) Recombinant human butyrylcholinesterase G390V, the fluoride-2 variant, expressed in Chinese hamster ovary cells, is a low affinity variant. J Biol Chem 268(19):14329–14341

Masson P, Xie W, Froment MT, Levitsky V, Fortier PL, Albaret C, Lockridge O (1999) Interaction between the peripheral site residues of human butyrylcholinesterase, D70 and Y332, in binding and hydrolysis of substrates. Biochim Biophys Acta 1433(1–2):281–293

Masson P, Xie W, Froment MT, Lockridge O (2001) Effects of mutations of active site residues and amino acids interacting with the

Omega loop on substrate activation of butyrylcholinesterase. Biochim Biophys Acta 1544(1–2):166–176
Nicolet Y, Lockridge O, Masson P, Fontecilla-Camps JC, Nachon F (2003) Crystal structure of human butyrylcholinesterase and of its complexes with substrate and products. J Biol Chem 278:41141–41147
Parrinello M, Rahman A (1981) Polymorphic transitions in single crystals: a new molecular dynamics method. J App Phys 52(12):7182–7190
Schwede T, Kopp J, Guex N, Peitsch MC (2003) SWISS-MODEL: an automated protein homology-modeling server. Nucleic Acids Res 31:3381–3385
Shao Y, Molnar LF, Jung Y, Kussmann J, Ochsenfeld C, Brown ST, Head-Gordon M (2006) Advances in methods and algorithms in a modern quantum chemistry program package. Phys Chem 8(27):3172–3191
Silva AWS, Vranken WF (2012) ACPYPE—AnteChamber PYthon Parser interfacE. BMC Res Notes 23:5:367
Sitkoff D, Sharp KA, Honig B (1994) Accurate calculation of hydration free energies using macroscopic solvent models. J Phys Chem 98(7):1978–1988
Suárez D, Field MJ (2005) Molecular dynamics simulations of human butyrylcholinesterase. Proteins 59:104–117
Suárez D, Díaz N, Fontecilla-Camps J, Field MJ (2006) A computational study of the deacylation mechanism of human butyrylcholinesterase. Biochemistry 45:7529–7543
Thomsen R, Christensen MH (2006) MolDock: a new technique for high-accuracy molecular docking. J Med Chem 49:3315–3321
Trott O, Olson AJ (2010) AutoDock Vina: improving the speed and accuracy of docking with a new scoring function, efficient optimization, and multithreading. J Comput Chem 31:455–461
Van der Spoel D, Lindahl E, Hess B, van Buuren AR, Apol E, Meulenhoff PJ, Tieleman DP, Sijbers ALTM, Feenstra KA, van Drunen R, Berendsen HJC (2005) GROMACS user manual version 3.3. http://www.gromacs.org. Accessed 12 Mar 2019
Vilanova E, Barril J, Carrera V, Pellin MC (1990) Soluble and particulate forms of the organophosphorus neuropathy target esterase in hen sciatic nerve. J Neurochem 55(4):1258–1265
Vorobjev YN, Almagro JC, Hermans J (1998) Discrimination between native and intentionally misfolded conformations of proteins: ES/IS, a new method for calculating conformational free energy that uses both dynamics simulations with an explicit solvent and an implicit solvent continuum model. Proteins 32(4):399–413
Wiesner J, Kříž Z, Kuča K, Jun D, Koča J (2010) Why acetylcholinesterase reactivators do not work in butyrylcholinesterase. J Enzyme Inhib Med Chem 25(3):318–322
Wong KKK, Ngo JC, Liu S, Lina H, Hu C, Shaw PC, Wan DC (2010) Interaction study of two diterpenes, cryptotanshinone and dihydrotanshinone,to human acetylcholinesterase and butyrylcholinesterase by molecular docking and kinetic analysis. Chem Biol Interact 187:335–339

Publisher's Note Springer Nature remains neutral with regard to jurisdictional claims in published maps and institutional affiliations.